Journal of Power Sources 267 (2014) 566–575

Contents lists available at ScienceDirect

Journal of Power Sources

journal homepage: www.elsevier.com/locate/jpowsour

Control design for robust tracking and smooth transition in power systems with battery/supercapacitor hybrid energy storage devices☆

Hoeguk Jung, Haifeng Wang, Tingshu Hu*

Department of Electrical and Computer Engineering, University of Massachusetts, Lowell, MA 01854, United States

HIGHLIGHTS

- Control design problems addressed for battery/supercapacitor hybrid energy systems.
- Active current control implemented via two bi-directional buck–boost converters.
- Controller designed via efficient numerical optimization.
- Robust tracking achieved for regulating battery current and dc-bus voltage.
- Smooth transition achieved during load switch.

ARTICLE INFO

Article history:
Received 7 February 2014
Received in revised form
27 March 2014
Accepted 7 May 2014
Available online 2 June 2014

Keywords:
Battery
Supercapacitor
Hybrid energy storage
dc–dc Converter
Robust tracking
Smooth transition

ABSTRACT

This paper considers some control design problems in a power system driven by battery/supercapacitor hybrid energy storage devices. The currents in the battery and the supercapacitor are actively controlled by two bidirectional buck–boost converters. Two control objectives are addressed in this paper: one is to achieve robust tracking of two reference variables, the battery current and the load voltage, the other is to achieve smooth transition of these variables during load switch. Based on the state-space averaged model we newly developed, the control design problems are converted into numerically efficient optimization problems with linear matrix inequality (LMI) constraints. An experimental system is constructed to validate the control design methods.

1. Introduction

Batteries and supercapacitors have been combined into hybrid energy storage devices which have both the high energy density of the batteries and the high power density of the supercapacitors. The main function of supercapacitors in a hybrid energy storage system is to provide high currents during hard transience such as motor start, which is essential to protecting the batteries from fatal damages caused by over-discharge. Supercapacitors are also used to absorb excess current when wind/solar power is abundant, and to store energy from regenerative braking. The battery/supercapacitor hybrid energy storage systems have been widely used in electric, hybrid and plug-in hybrid electric vehicles, e.g., see Refs. [1–4]. They have also found applications in wind systems [5–7], communication systems [8], photovoltaic systems [9], and microgrids [10]. In some hybrid electric vehicle applications, the hybrid energy storage system also include fuel cells as one power source [11–13].

There are various configurations to combine batteries and supercapacitors. The advantage and disadvantage of each configuration are discussed in Refs. [3,14–16]. In Ref. [17], the performance of different configurations were compared via simulation on a stand along power system. The simplest configuration is to connect the battery and the supercapacitor in parallel. This will reduce the current stress of the battery but the two power sources need the same voltage and the power flow cannot be controlled. To achieve active control of currents, especially the current from the battery,

☆ Research supported by the National Science Foundation under grants ECCS-0925269, 1200152.

* Corresponding author. Tel.: +1 978 934 4374 (office); fax: +1 978 934 3027.
E-mail addresses: tingshu_hu@uml.edu, tingshu@gmail.com (T. Hu).

http://dx.doi.org/10.1016/j.jpowsour.2014.05.061
0378-7753/

dc–dc converters are needed to connect the power sources and the load or dc bus. In some configurations [18–21], one dc–dc converter is used to connect the battery and the supercapacitor.

The most commonly used configuration contains two bidirectional buck–boost converter connected in parallel at the load side, and fed by a battery and a supercapacitor respectively, see Fig. 1. The advantage of this configuration is that both the current from the battery and the current from the supercapacitor can be actively controlled. Such a configuration has been considered, for example, in Refs. [8,14,16,22]. Similar configurations have been used to combine fuel cells and supercapacitors, e.g., in Ref. [11], where the fuel cell is connected to the dc bus via a one-directional boost converter. In Ref. [23], three buck–boost converters were connected in parallel to combine three power sources. For the configuration in Fig. 1, different strategies have been proposed to actively control the current flow from the battery and the supercapacitor.

A common strategy is to use a certain power management algorithm to determine a reference current that is needed from the battery or the supercapacitor, then use decentralized reference tracking control, typically PI control, on each dc–dc converter to track the respective reference current. In Ref. [24], one algorithm was proposed for maximum efficiency and the other algorithm for minimal battery current to prolong the life span of batteries. In Ref. [16], a power management algorithm was proposed for minimization of the magnitude/fluctuation of the battery current and energy loss. In Ref. [25], three piecewise linear functions were proposed for allocating the battery current and supercapacitor current. Simulation results were generated to demonstrate the effectiveness of the allocation function under different operating conditions. In Ref. [10], several current allocation strategies were proposed by considering the power demand, the state of charge of the battery and the supercapacitor. In Ref. [22], three classical control loops were constructed to regulate the battery current, the output voltage and the supercapacitor voltage.

In most of the existing literature which considered similar configuration as in Fig. 1, the control design algorithms were focused on generating reference currents for the battery and the supercapacitor. It was generally assumed that a classical reference tracking loop would yield a required current from the battery or the supercapacitor. These control strategies do not consider the interaction among the control loops and the power loss in the circuit elements. In fact, the parallel dc–dc converters are coupled via the same dc-bus or load and have complex interactions. If the interactions among the different control loops are ignored, the transient behavior may not be desirable, such as with large overshoot or undershoot, which may damage the circuit parts. If the power loss is not carefully considered in the current allocation algorithm, the output power may be different than the desired power.

For better analysis and control of the coupled dc–dc converters, we need effective and faithful models for the whole power electronic system. Recently, we derived two state-space averaged models for the system in Ref. [26]. One for simulation and analysis of the open-loop system and the closed-loop system, and the other for control design. The advantage of the averaged models is the simplicity and that they have clear structure in terms of the two duty cycles. Furthermore, they are much faster for simulation than the SimPower models.

In this paper, we would like to address some control design problems for the typical configuration with two bidirectional dc–dc converters as in Fig. 1. A standard control problem in such power systems is to achieve reference tracking for some variables such as battery current, supercapacitor current, load voltage and load current. Since the hybrid energy storage system has two control inputs, the duty cycles of the two dc–dc converters, it should be able to track references for two circuit variables. One may still choose the battery current and the supercapacitor current as in some earlier works. In this paper, we will choose the battery current and the load voltage since the supercapacitor is playing a supporting role and it can supply or absorb almost any current as needed. After all, the state-of-health of the battery (which depends on its charging/discharging profiles) and the performance of the load are of high priority.

We will also address the problem of control design for smooth transition of some key variables during load switch. This will also help to protect the battery and to enhance the performance of the whole system.

It should be noted that this paper's control design methods can be combined with the existing current allocation strategies. With the reference currents generated by any of the existing method, the tracking control can be implemented by the controllers designed by our optimization algorithm.

This paper is organized as follows. In Section 2, we describe the circuit system and briefly summarize the two state-space averaged models developed in Ref. [26]. In Section 3, two design objectives

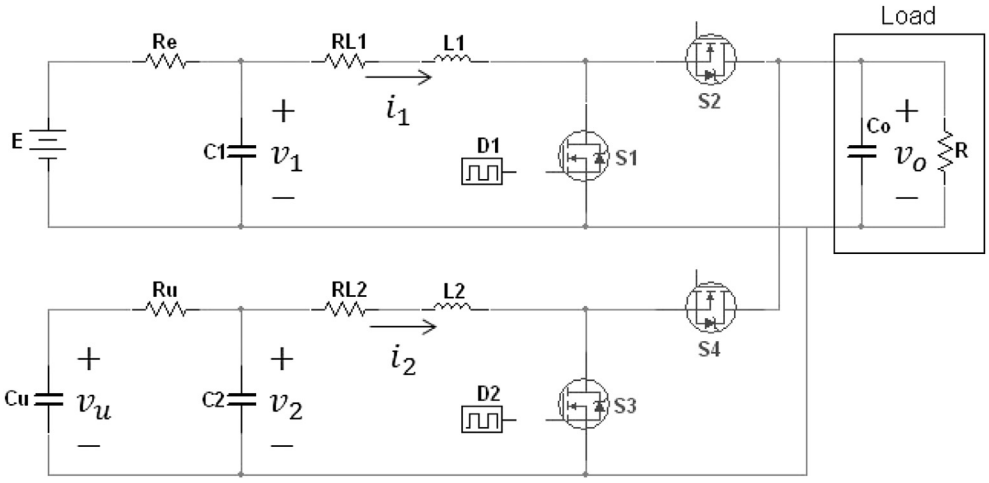

Fig. 1. Parallel topology of the buck–boost converters.

are addressed: One is to achieve robust tracking and the other is to achieve robust tracking with smooth transition during load switch. Both design problems are formulated as optimization problems with linear matrix inequality constraints. In Section 4, the design methods are applied to an experimental system and yield two state feedback laws. The performances of the system under these feedback laws are validated via the averaged model and the SimPower Model. Section 5 validates the effectiveness of the control design methods on an experimental system. Section 6 concludes this paper.

2. Description of the power system and two state-space averaged models

The circuit diagram of the hybrid energy storage system is illustrated in Fig. 1. It consists of two standard bi-directional buck–boost converter connected in parallel at the load side, and fed by a battery and a supercapacitor respectively. The load is represented by a resistor for simplicity, as in some literature, e.g., [27]. In Ref. [22], the load is represented by a current source. In electrical vehicle applications, the load is typically an inverter followed by a motor [18]. The inverter and the motor can be made equivalent to a resistor whose resistance varies within a certain range. During motor start, the equivalent load resistance is much smaller than in other operating conditions.

For simplicity of presentation, the battery and the supercapacitor are described with models which only include parasitic series resistances R_e and R_u, respectively. More comprehensive models can be considered, such as adding one or two pairs of parallel resistor and capacitor for the battery, as in Refs. [28,29], and using a second-order RC circuit to describe a supercapacitor, as in Refs. [1,27]. In Ref. [28], an algebraic method was developed for identifying the circuit parameters of a battery.

The two MOSFETs S_1 and S_2 operate synchronously, when one is off, the other is on. Similarly with S_3 and S_4. Let the duty cycle for the on state of S_1 be D_1 and the duty cycle for the on-state of S_3 be D_2. The on-resistances for S_1, S_2, S_3, S_4 are denoted as $R_{\text{on},1}$, $R_{\text{on},2}$, $R_{\text{on},3}$, $R_{\text{on},4}$, respectively. Based on the state-space averaging method, we derived two state-space averaged models in Ref. [26] for the hybrid energy storage system: a 6th order model for simulation and a 5th order model for control design. If more complex models for the battery and the supercapacitor are considered, the method in Ref. [26] will yield higher order state-space models, with matrices of the same structure but larger dimensions.

For the 6th order model, the voltage v_u of the supercapacitor is considered as a state variable in addition to v_1, v_2, i_1, i_2 and v_o, as marked in Fig. 1. The 6 state variables are arranged in a state vector $\zeta = [\,v_1 \quad v_2 \quad v_u \quad i_1 \quad i_2 \quad v_o\,]^T$. The averages of the state variables over one switching period are denoted as $\bar{v}_1$, $\bar{v}_2$, $\bar{v}_u$, $\bar{i}_1$, $\bar{i}_2$, $\bar{v}_o$, respectively. The average of the state vector ζ is denoted as $\bar{\zeta}$.

The 6th order averaged model is

$$\dot{\bar{\zeta}} = \left(\widehat{A}_0 + \widehat{A}_1 D_1 + \widehat{A}_2 D_2\right)\bar{\zeta} + B_e E \tag{1}$$

where E is the open circuit voltage of the battery. The matrices $\widehat{A}_0$, $\widehat{A}_1$, $\widehat{A}_2$ and B_e depend on circuit parameters. Detailed structure and expression for these matrices can be found in Ref. [26].

It is commented in Ref. [26] that the 6th order model (1) is suitable for simulation of the open-loop system under constant duty cycles D_1 and D_2, as well as for the closed-loop system under particular control strategies. However, it is not suitable for steady-state analysis or control design. The main reason is that, its equilibrium point, where $\dot{\bar{\zeta}} = 0$, is not a useful operating condition since it implies $\mathrm{d}\bar{v}_u/\mathrm{d}t = 0$. Under this condition, the supercapacitor is not supplying/absorbing current and thus not assisting the power system. In general application, the supercapacitor is used for discharging high current for only a brief moment and will be recharged soon. The high current discharging mode is very important but will not last long enough to reach a steady state.

For control design (stabilization or tracking), we need to consider a nominal working condition and to derive a perturbation model around this nominal condition, which has to be a steady state (or an equilibrium point). To handle this situation, we may replace the supercapacitor C_u with an ideal voltage source E_u for the purpose of control design and for determining the input/output current or voltage after the fast transience of the dc–dc converters. We can ignore the dynamics of the supercapacitor even when it is discharging at a high current, since the decrease of its voltage is still slow as compared to the fast dynamics of other elements.

In this respect, a 5th order averaged model were derived in Ref. [26]. Denote the state variable as $\zeta = [\,v_1 \quad v_2 \quad i_1 \quad i_2 \quad v_o\,]^T$, and the averaged state as $\bar{\zeta}$. Denote

$$\bar{A}_{11} = \begin{bmatrix} -\dfrac{1}{R_e C_1} & 0 \\ 0 & -\dfrac{1}{R_u C_2} \end{bmatrix},\ \bar{A}_{12} = \begin{bmatrix} -\dfrac{1}{C_1} & 0 & 0 \\ 0 & -\dfrac{1}{C_2} & 0 \end{bmatrix}$$

$$\bar{A}_{21} = \begin{bmatrix} \dfrac{1}{L_1} & 0 \\ 0 & \dfrac{1}{L_2} \\ 0 & 0 \end{bmatrix},\ \bar{B}_e = \begin{bmatrix} \dfrac{1}{R_e C_1} & 0 \\ 0 & \dfrac{1}{R_u C_2} \\ 0 & 0 \\ 0 & 0 \\ 0 & 0 \end{bmatrix}$$

$$W_0 = \begin{bmatrix} -\dfrac{R_{L1} + R_{\text{on}2}}{L_1} & 0 & -\dfrac{1}{L_1} \\ 0 & -\dfrac{R_{L2} + R_{\text{on}4}}{L_2} & -\dfrac{1}{L_2} \\ \dfrac{1}{C_o} & \dfrac{1}{C_o} & -\dfrac{1}{RC_o} \end{bmatrix} \tag{2}$$

$$W_1 = \begin{bmatrix} \dfrac{R_{\text{on}2} - R_{\text{on}1}}{L_1} & 0 & \dfrac{1}{L_1} \\ 0 & 0 & 0 \\ -\dfrac{1}{C_o} & 0 & 0 \end{bmatrix} \tag{3}$$

$$W_2 = \begin{bmatrix} 0 & 0 & 0 \\ 0 & \dfrac{R_{\text{on}4} - R_{\text{on}3}}{L_2} & \dfrac{1}{L_2} \\ 0 & -\dfrac{1}{C_o} & 0 \end{bmatrix} \tag{4}$$

and

$$\bar{A}_0 = \begin{bmatrix} \bar{A}_{11} & \bar{A}_{12} \\ \bar{A}_{21} & W_0 \end{bmatrix},\ \bar{A}_1 = \begin{bmatrix} 0 & 0 \\ 0 & W_1 \end{bmatrix},\ \bar{A}_2 = \begin{bmatrix} 0 & 0 \\ 0 & W_2 \end{bmatrix}$$

Denote $V_e = \begin{bmatrix} E \\ E_u \end{bmatrix}$, then the 5th order averaged model is

$$\dot{\bar{\xi}} = \left(\bar{A}_0 + \bar{A}_1 D_1 + \bar{A}_2 D_2\right)\bar{\xi} + \bar{B}_e V_e \tag{5}$$

3. Control design for robust reference tracking and smooth transition

3.1. Converting the tracking problem to a stabilization problem

Strictly speaking, stabilization for the original hybrid energy storage system as described Fig. 1 and the 6th order averaged model (1) is not a meaningful problem. This is because stability or tracking is defined in terms of a useful equilibrium point, where you want the state of the system to stay there for a desirable time period. The equilibrium point of the 6th order model is useless since the derivative of the supercapacitor voltage must be 0, which means that its current is 0. However, we need a perturbation model around the equilibrium point for control design. So we have to use the 5th order model, which is obtained by excluding the voltage of the supercapacitor from the state of the 6th order model, for control design. Instead, the supercapacitor voltage is considered as a voltage source E_u, which is allowed to be varying "slowly" within a certain range.

The controller designed for the 5th order model should work for the 6th order model for reasonably long time period. The reasons include: 1) the controller designed by our LMI-based method is robust, which means that it can tolerate some uncertainty or change of parameters; 2) The change of supercapacitor voltage is very slow as compared to the transient response of other state variables. The sizing of the supercapacitor should take into account this requirement.

Since there are two control inputs D_1 and D_2, a practical control objective is to track the reference for a two-dimensional output, e.g., $\bar{y} = \begin{bmatrix} \bar{i}_b \\ \bar{i}_{sc} \end{bmatrix}$, $\begin{bmatrix} \bar{i}_1 \\ \bar{v}_o \end{bmatrix}$. In general, consider $\bar{y} = C\bar{\xi}$ where C is a matrix of two rows.

For safety and efficiency, the duty cycles D_1, D_2 are restricted in a subset of (0, 1). For this reason and other circuit limitations, we make the following observations:

1. For the 5th order model where the supercapacitor is replaced with an ideal voltage source E_u, for each output reference $\bar{y}_{ref}$, there is a certain range for the source voltages (E, E_u) where tracking is possible.
2. According to charge and energy conservation principles, for the original 6th order system with supercapacitor, generic tracking can only last for a finite time period, beyond which the supercapacitor voltage will drop (or rise) out of the range where $\bar{y}_{ref}$ can be tracked.

To see item 1, we note that $\bar{v}_o$ has to be greater than both E and E_u and the gain from E and E_u to v_o is limited by the load resistance and the range of duty cycles. For item 2, we note that in a real hybrid energy storage system, the reference $\bar{y}_{ref}$ is recalculated after a while according the load requirement, the state of charge of the battery and the state of charge of the supercapacitor. During heavy load period, the supercapacitor supplies most of the current and its voltage decreases quickly. This period does not (and cannot) last long. During light load period, the supercapacitor is recharged. The charging rate depends on the battery current. This period can last much longer than the heavy load period. But if the same operation mode is allowed to last forever, the supercapacitor voltage will rise out of the limit.

Item 2 in the above statements further justifies the use of the 5th order model for control design instead of the 6th order model. In this paper we focus on the control of the fast dynamics characterizing the power converters, neglecting the above-mentioned supercapacitor sizing and voltage regulation. Slow variation of the supercapacitor voltage will be regarded as a model uncertainty to be handled by the robust feedback controller.

Combining the 5th order model (5) with an output of interest, we obtain

$$\begin{aligned} \dot{\bar{\xi}} &= \left(\bar{A}_0 + \bar{A}_1 D_1 + \bar{A}_2 D_2\right)\bar{\xi} + \bar{B}_e V_e \\ \bar{y} &= C\bar{\xi} \end{aligned} \tag{6}$$

where $V_e = \begin{bmatrix} E \\ E_u \end{bmatrix}$ and C is a 2 by 5 matrix depending on the circuit variables to be tracked. For example,

$$C = \begin{bmatrix} 0 & 0 & 1 & 0 & 0 \\ 0 & 0 & 0 & 0 & 1 \end{bmatrix} \tag{7}$$

implies $\bar{y} = \begin{bmatrix} \bar{i}_1 \\ \bar{v}_o \end{bmatrix}$.

For a particular pair (E, E_u), a reference $\bar{y}_{ref}$ can be tracked if there exist $D_1, D_2 \in (0, 1)$ such that $C\bar{\xi}_{ss} = \bar{y}_{ref}$ where $\bar{\xi}_{ss}$ is the steady-state satisfying $\dot{\bar{\xi}}_{ss} = 0$, i.e.,

$$\bar{\xi}_{ss} = -\left(\bar{A}_0 + \bar{A}_1 D_1 + \bar{A}_2 D_2\right)^{-1} \bar{B}_e V_e$$

Before designing a control law, we need to choose a suitable nominal operating condition which involves the following variables: $V_{e0} = \begin{bmatrix} E_0 \\ E_{u0} \end{bmatrix}$, D_{10}, D_{20}, and $\bar{\xi}_{ss,0}$ satisfying

$$\bar{\xi}_{ss,0} = -\left(\bar{A}_0 + \bar{A}_1 D_{10} + \bar{A}_2 D_{20}\right)^{-1} \bar{B}_e V_{e0} \tag{8}$$

Next, we need a perturbation model around this nominal condition. Define $x = \bar{\xi} - \bar{\xi}_{ss,0}$, $y = \bar{y} - C\bar{\xi}_{ss,0}$, $u_1 = D_1 - D_{10}$, $u_2 = D_2 - D_{20}$ and $u = \begin{bmatrix} u_1 \\ u_2 \end{bmatrix}$. Also denote

$$A_0 = \bar{A}_0 + \bar{A}_1 D_{10} + \bar{A}_2 D_{20},\ B = \begin{bmatrix} \bar{A}_1 \bar{\xi}_{ss,0} & \bar{A}_2 \bar{\xi}_{ss,0} \end{bmatrix}$$

then by plugging $\bar{\xi} = x + \bar{\xi}_{ss,0}$, $D_1 = u_1 + D_{10}$ and $D_2 = u_2 + D_{20}$ into (6) and applying (8), we obtain the following perturbation model:

$$\begin{aligned} \dot{x} &= A_0 x + \bar{A}_1 x u_1 + \bar{A}_2 x u_2 + Bu + \bar{B}_e(V_e - V_{e0}) \\ y &= Cx \end{aligned} \tag{9}$$

We may design a feedback law to stabilize the system (9) under the nominal condition where $V_e = V_{e0}$. However, it is almost always true that $V_e \neq V_{e0}$ since the battery voltage or the supercapacitor voltage are always changing. Furthermore, the desired value for the output is also changed frequently and the load resistance is not a constant.

A common strategy to achieve robust reference tracking in the presence of uncertainties, is to integrate the tracking error $e = y - y_{ref}$ and include the integration as a new state variable. Here y_{ref} is a two dimensional vector. It is generally different than $C\bar{\xi}_{ss,0}$, the output at the nominal condition. To be specific, define

$$x_a = \int \left(y - y_{ref}\right) dt = \int \left(Cx - y_{ref}\right) dt \tag{10}$$

and define the augmented state as $x_w := \begin{bmatrix} x \\ x_a \end{bmatrix}$. Also define the following matrices:

$$\overline{A}=\begin{bmatrix}A_0 & 0\\ C & 0\end{bmatrix},\ \overline{A}_{b1}=\begin{bmatrix}\overline{A}_1 & 0\\ 0 & 0\end{bmatrix},\ \overline{A}_{b2}=\begin{bmatrix}\overline{A}_2 & 0\\ 0 & 0\end{bmatrix}$$
$$\overline{B}=\begin{bmatrix}B\\ 0\end{bmatrix},\ g=\begin{bmatrix}\overline{B}_e(v_e-v_{e0})\\ -y_{\text{ref}}\end{bmatrix}$$

where the zero blocks have compatible dimensions. Then x_w satisfies

$$\dot{x}_w=\overline{A}x_w+\overline{A}_{b1}x_wu_1+\overline{A}_{b2}x_wu_2+\overline{B}u+g \tag{11}$$

Here $x_w\in\mathbb{R}^7$ includes the perturbations of the voltages of three capacitors C_1, C_2, C_o, the two inductor currents, and two integrator outputs. This turns the reference tracking problem into a standard stabilization problem: design a feedback control law $u=f(x_w)$ which stabilizes (11) with a large stability region, under the nominal condition $g=0$, and under the control constraint $D_1, D_2\in(0,1)$. If the system drifts away from the nominal working condition and goes to another equilibrium point, each state variable, in particular, the integral x_a, will still reach a steady state. This means that $y-y_{\text{ref}}$ must go to zero and the output y is regulated to the desired value y_{ref}.

In what follows, we design a stabilizing feedback for (11) under input constraint by extending the method in Refs. [29,30] for systems with one input to systems with two inputs.

3.2. State feedback design for robust tracking via LMI optimization

Let us first deal with the input constraints. In general, assume $D_j\in[D_{j\min},\ D_{j\max}]\subset[0,\ 1],\ j=1,\ 2$. This corresponds to $D_{j\min}-D_{j0}\le u_j\le D_{j\max}-D_{j0}$. Denoting $u_{mj}=D_{j0}-D_{j\min}$, $u_{pj}=D_{j\max}-D_{j0}$, the input constraints can be expressed as

$$-u_{mj}\le u_j\le u_{pj},\ j=1,\ 2 \tag{12}$$

The input constraint will be enforced via some saturation functions defined as follows. For $j=1,2$

$$\text{sat}(u_j)=\begin{cases}u_{pj} & u_j>u_{pj}\\ u_j & u_j\in[-u_{mj},u_{pj}]\\ -u_{mj} & u_j<-u_{mj}\end{cases}$$

with some abuse of notation, for $u\in\mathbf{R}^2$, denote $\text{sat}(u)=\begin{bmatrix}\text{sat}(u_1)\\ \text{sat}(u_2)\end{bmatrix}$

We will consider a simple saturated state feedback $u=\text{sat}(Kx)$. Under this state feedback and the nominal working condition, we obtain the following closed-loop system:

$$\dot{x}_w=\left(\overline{A}+\overline{A}_{b1}\text{sat}(k_1x_w)+\overline{A}_{b2}\text{sat}(k_2x_w)\right)x_w+\overline{B}\text{sat}(Kx_w) \tag{13}$$

The nonlinear matrices $\overline{A}_{b1}\text{sat}(k_1x_w)$ and $\overline{A}_{b2}\text{sat}(k_2x_w)$ will be handled with inclusion and the term $\overline{B}\text{sat}(Kx_w)$ will be handled by the method in Ref. [31]. Define

$$\tilde{A}_1=\overline{A}-u_{m1}\overline{A}_{b1}-u_{m2}\overline{A}_{b2},\ \tilde{A}_2=\overline{A}-u_{m1}\overline{A}_{b1}+u_{p2}\overline{A}_{b2}$$
$$\tilde{A}_3=\overline{A}+u_{p1}\overline{A}_{b1}-u_{m2}\overline{A}_{b2},\ \tilde{A}_4=\overline{A}+u_{p2}\overline{A}_{b1}+u_{p2}\overline{A}_{b2}$$

Then x_w satisfies

$$\dot{x}_w\in\text{co}\left\{\tilde{A}_ix_w+\overline{B}\text{sat}(Kx_w),\ i=1,\ \ldots,\ 4\right\} \tag{14}$$

where co{X} denote the convex hull of the set X. In particular,

$$\text{co}\{a,b,c,d\}=\{\gamma_1a+\gamma_2b+\gamma_3c+\gamma_4d:\Sigma\gamma_i=1,\ \gamma_i\ge0\}$$

By applying the methods reported in Refs. [30–32], to the differential inclusion (14), with slight generalization, we can design a feedback gain K to achieve the maximal stability region under the input constraint (12). Note that the size of the stability region is closely related to the robustness against parameter change and the range of references that can be tracked.

The design methods are developed based on Lyapunov function and some theory on set invariance, which are powerful tools for dealing with input and state constraints. The stabilization problem can be converted into a numerically efficient optimization problem with linear matrix inequality (LMI) constraints. Detailed ideas and explanations can be found in Refs. [30–32].

For the particular system (14) under input constraint (12), the design objective for achieving the maximal stability region can be cast into the following optimization problem:

$$\begin{aligned}&\inf_{Q>0,Y,\gamma}\ \gamma\\ &\text{s.t.}\quad a)\tilde{A}_iQ+Q\tilde{A}_i^T+\overline{B}Y+Y^T\overline{B}^T<-2\eta Q,\ \ i=1,\ldots,4\\ &\qquad b)\begin{bmatrix}\min\left(u_{mj}^2,u_{pj}^2\right) & Y_j\\ Y_j^T & Q\end{bmatrix}\ge0,\ j=1,2\\ &\qquad c)\begin{bmatrix}Q & I\\ I & \gamma I\end{bmatrix}\ge0\end{aligned} \tag{15}$$

where Y_1, Y_2 are the two rows of Y and $\eta>0$ is an optimization parameter that can be chosen by experience. In general, larger η would result in larger elements in the feedback gain K and faster response. However, if the elements in K are too large, the control input will be easily saturated, which may yields small stability region. Thus we usually have to adjust η after some simulation or experiment on the closed-loop system.

The matrix variables to be optimized are $Q\in\mathbb{R}^{7\times7}$ and $Y\in\mathbb{R}^{2\times7}$, while the other matrices are constants obtained from the averaged model following some steps. The optimization problem can be easily solved with the "mincx" solver (minimizing linear objective under LMI constraints) in the LMI toolbox of MATLAB. After Q and Y are solved, the feedback matrix is obtained as $K=YQ^{-1}$.

The feedback control designed via the LMI optimization problem will always allow certain ranges of parameters where robust tracking can be achieved. These ranges can also be estimated via some optimization problem but the results may be conservative. The averaged model will provide an easy and fast approach for verifying robustness within a certain parameter range.

3.3. State feedback design for smooth transition

Simulation and initial experimental results showed that the controller designed for robust reference tracking may yield unsatisfactory transient performances. For example, when the load is switched from 200 Ω to 4 Ω, there is significant undershoot for the load voltage and large overshoot for the battery current (see Fig. 2). When the load is switched from heavy to light, there are significant overshoot for load voltage and undershoot for battery current. These overshoots and undershoots will have adverse effects to the battery, the load performance and the reliability of the whole system.

To reduce the overshoot/undershoot of the outputs, we first need some tools to evaluate such transient performances. Such tools were developed in Ref. [33], where the overshoot/undershoot is evaluated via invariant ellipsoids. Invariant ellipsoid is a powerful tool based on Lyapunov theory. If there is an invariant set S that contains all the possible initial conditions, then the state trajectories will stay within the invariant set and we can estimate the maximal/minimal output via the invariant set. Suppose that the set of initial conditions is bounded by a ball $X_0=\{x\in\mathbf{R}^n:x^Tx\le r_0^2\}$,

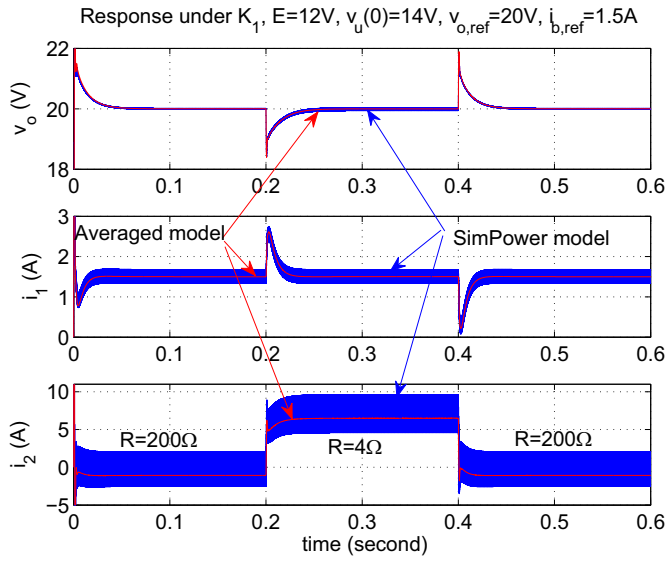

Fig. 2. Response to load switch: $E = 12$ V, $v_u(0) = 14$ V, feedback gain K_1.

and the invariant ellipsoid is $\varepsilon = \{x \in \mathbf{R}^n : x^T Q^{-1} x \le 1\}$. The relationship $X_o \subset \varepsilon$ can be described by the matrix inequality $Q \ge r_0^2 I_n$.

Suppose that we need to evaluate the maximal $y_1 = C_1 x$ under the condition $x_0 \in X_0$. Assume $X_0 \subset \varepsilon$ and ε is an invariant set. A bound on the maximal y_1 can be computed as

$$\inf \gamma_1^2, \text{s.t.} \begin{bmatrix} \gamma_1^2 & C_1 Q \\ Q C_1^{\mathrm{T}} & Q \end{bmatrix} \ge 0 \tag{16}$$

To design a state feedback law with minimal overshoot for a certain output, we just need to impose the LMI constraint in (16) together with the constraints in (15), with the objective of minimizing γ_1 under a guaranteed γ.

For the particular system in this paper, we need to reduce the overshoot/undershoot of two outputs: $y_1 = C_1 x$ as the battery current and $y_2 = C_2 x$ as the load voltage. We use γ_1 and γ_2 to denote the magnitudes of y_1 and y_2 respectively.

Since these two outputs may have conflict, we can use a weighting coefficient w and consider a combined measure $\gamma_1^2 + w\gamma_2^2$. The optimization problem can be described as

$$\begin{aligned} &\inf_{Q>0, Y, \gamma_1, \gamma_2} \ \gamma_1^2 + w\gamma_2^2 \\ &\text{s.t.} \quad a) \tilde{A}_i Q + Q \tilde{A}_i^T + \overline{B} Y + Y^T \overline{B}^T < -2\eta Q, \ \ i = 1, \ldots, 4 \\ &\qquad b) \begin{bmatrix} \min\left(u_{mj}^2, u_{pj}^2\right) & Y_j \\ Y_j^T & Q \end{bmatrix} \ge 0, \ j = 1, 2 \\ &\qquad c) \begin{bmatrix} Q & I \\ I & \gamma I \end{bmatrix} \ge 0 \\ &\qquad d) \begin{bmatrix} \gamma_1^2 & C_1 Q \\ Q C_1^{\mathrm{T}} & Q \end{bmatrix} \ge 0, \ \begin{bmatrix} \gamma_2^2 & C_2 Q \\ Q C_2^{\mathrm{T}} & Q \end{bmatrix} \ge 0. \end{aligned} \tag{17}$$

As compared with the optimization problem (15), the new constraint d) is added with an objective of minimizing $\gamma_1^2 + w\gamma_2^2$. To ensure a certain robustness on the tracking performance, we choose an appropriate value for γ.

Note that there are three parameters, η, γ and w, that need to be chosen before optimization. Since the relationship between these parameters and the output performances are complex, we may try different combinations and then use simulation to decide which resulting controller is the best.

4. Control design for an experimental system and simulation results

4.1. Open-loop system description

An experimental system was constructed for the hybrid energy storage configuration as described in Fig. 1. The fixed parameters are provided in Table 1.

The load resistance R is variable. A time varying profile of the resistance R can be constructed to mimic the different operation modes of an electric machine. In our simulation and experiment, we used a simple switch to change the resistance between a few ohms (heavy load) and several hundred ohms (light load). The battery is a lead-acid one rated 12 V, 13 Ah. Its open circuit voltage varies between 11.6 V and 12.6 V, corresponding to 10% and 100% state of charge, respectively. The supercapacitor consists of two parallel ones rated 58 F, 16.2 V with serial resistance 0.022 Ω. For control design, the supercapacitor was considered as an ideal voltage source varying between 12 V and 16 V. It should be clarified that in both simulation and experiment, the supercapacitor was used. The simulation was carried out with both SimPower and Simulink with the 6th order averaged model (1) instead of the 5th order model.

The control objective is to keep the load voltage at a desired value, e.g., 20 V, for both heavy load and light load conditions. To ensure safe discharging of the battery, we would like to keep the battery current at a certain constant below 3 A. The reference value for the battery current can be changed according to the state of charge. Thus we need to design a controller for tracking the output $\overline{y} = \begin{bmatrix} i_1 \\ v_o \end{bmatrix}$.

The nominal working condition is chosen based on the control objective and the rating of the battery and the supercapacitor. The nominal battery voltage is chosen as $E_0 = 12$ V. For control design, the nominal voltage for the ideal voltage source in place of the supercapacitor is chosen as $E_{u0} = 14$ V. For the load resistance, we focus on the heavy load condition thus we choose $R_0 = 4$ Ω. The nominal condition for the output is chosen as $\overline{y}_0 = \begin{bmatrix} 3 \\ 20 \end{bmatrix}$. The unique duty cycles (D_1, D_2) that produce this nominal output is $(D_{10}, D_{20}) = (0.447, 0.337)$ and the steady state for the 5th order averaged model is $\overline{\xi}_{\mathrm{ss},0} = [11.88 \quad 13.94 \quad 5.03 \quad 20]^T$. Using these conditions, a perturbation model can be computed.

For the duty cycle, we impose the restriction $D_1, D_2 \in [0, 0.8]$. The lower bound 0 and upper bound 0.8 are used to compute $u_{m1} = 0.447$, $u_{p1} = 0.353$, $u_{m2} = 0.337$, $u_{p2} = 0.463$.

4.2. Controller for robust tracking and simulation

First, we found the feedback gain K to achieve robust tracking. By solving (15) with different η, we can obtain a family of feedback gains K. Here is a feedback gain corresponding to $\eta = 50$:

$$K_1 = \begin{bmatrix} -0.0005 & -0.0000 \\ 0.0000 & -0.0000 \\ -0.0082 & -0.0001 \\ 0.0000 & -0.0002 \\ 0.0007 & -0.0009 \\ -2.8254 & 0.6908 \\ -1.9620 & -2.8779 \end{bmatrix}^T$$

This feedback gain was applied to both the averaged model and the SimPower model (with switching frequency 20 kHz). The nominal reference $\overline{y}_{\mathrm{ref}} = \begin{bmatrix} 3 \\ 20 \end{bmatrix}$ was successfully tracked in both models.

Table 1
Circuit parameters.

Symbol	Description	Quantity	Unit
L_1	Battery side inductance	680	[μH]
R_e	Battery series resistance	0.04	[Ω]
R_{L1}	Inductor series resistance	0.25	[Ω]
C_1	Battery side filter capacitance	1	[mF]
L_2	Supercapacitor side inductance	39	[μH]
R_u	Supercapacitor serial resistance	0.011	[Ω]
R_{L2}	Inductor series resistance	0.114	[Ω]
C_2	Supercapacitor side filter capacitance	0.22	[mF]
C_{sc}	Supercapacitor capacitance	116	[F]
R_{on}	MOSFET on-resistance	0.021	[Ω]
C	Load side capacitance	1	[mF]

It should be noted that the simulation with the averaged model is much faster than that by the SimPower model. For the averaged model, the sampling time can be chosen as 10^{-4} s. For the SimPower model, the sampling time has to be much smaller than the switching period. Generally, there should be about 25 or more samples within a switching period. For a 20 kHz switching frequency, the sampling period for the SimPower model needs to be 2×10^{-6} s. For example, to run a simulation of 0.6 s as in Figs. 2–5, the averaged model requires 18 s, while the SimPower model requires 960 s. Thus the averaged model can save a lot of time for determining the range of parameters for which tracking is achievable. If tracking is successful for a particular set of parameters by the averaged model, we then use SimPower model to validate it.

To validate the robustness of the tracking performance, we changed the load resistance R, the reference values for the output y_{ref}, the battery voltage E and the initial voltage of the supercapacitor $v_u(0)$ and run the simulation.

Simulation results showed that robust tracking can be achieved within a large range of parameters. For example, with $R = 4\ \Omega$ and $\bar{y}_{\text{ref}} = \begin{bmatrix} 1.5 \\ 20 \end{bmatrix}$, the tracking can be achieved for $E \in [11,\ 19]$ V, $v_u(0) \in [9,\ 19]$ V. For larger resistance R, larger ranges for E and $v_u(0)$ are allowed. If R is reduced to 2 Ω, then the source voltages cannot be too low: $E \geq 11$ V, $v_u(0) \geq 10.6$ V.

Fig. 2 shows the tracking performance when the load switches between light and heavy, with $\bar{y}_{\text{ref}} = \begin{bmatrix} 1.5 \\ 20 \end{bmatrix}$. Both the battery voltage E and the initial supercapacitor voltage $v_u(0)$ were set at the nominal value, 12 V and 14 V, respectively. The response by the averaged model is plotted with red curves (in the web version) and the response by the SimPower model is plotted with blue curves. For all the variables v_o, i_1, and i_2 by the SimPower model, the curves are saw-toothed with switching frequency 20 kHz. Thus they look like solid bands and the width of the band shows the magnitude of ripple. For the output voltage v_o, the band is thin and the ripple is small. The ripple of the current i_1 is visible but much smaller than the ripple of i_2, whose peak-to-peak value is nearly 5 A.

During the first 0.2 s, the load $R = 200\ \Omega$; from 0.2 to 0.4 s, $R = 4\ \Omega$; from 0.4 to 0.6 s, $R = 200\ \Omega$. The battery current i_b is similar to i_1 but with smaller ripples due to the filter capacitance C_1. Also, the supercapacitor current i_{sc} is similar to i_2 but with smaller ripples. During light load period, the supercapacitor absorbed current, during heavy load period, it supplied more than 5 A of current. Both the inductor current i_1 and the load voltage v_o were tracked under switching load.

Fig. 3 shows the response to load switch under the same feedback gain K_1 and reference $\bar{y}_{\text{ref}} = \begin{bmatrix} 1.5 \\ 20 \end{bmatrix}$, but E is reduced to 11 V and $v_u(0)$ is reduced to 9 V. The reference is still tracked. The most visible difference from Fig. 3, is that i_2 is significantly increased during the heavy load period. The steady state i_1 is kept at 1.5 A as intended. The other difference is that the overshoot and undershoot of i_1 and v_o are increased.

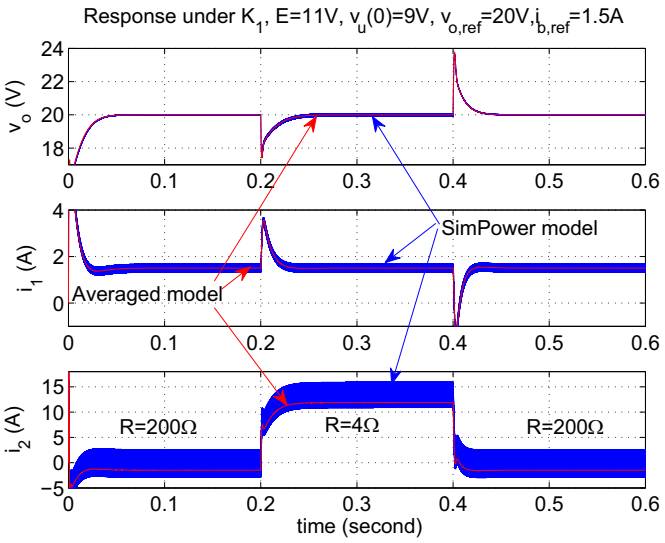

Fig. 3. Response to load switch: $E = 11$ V, $v_u(0) = 9$ V, feedback gain K_1.

Comparing Figs. 3 and 2, we can see that the battery current and the output voltage are very similar under different state of charge of the power sources. The supercapacitor supplies necessary power to protect the battery and to maintain the desired output power.

Although robust tracking is achieved by the feedback gain K_1, the transient dynamics during load switch is not satisfactory. The overshoot and undershoot of v_o are nearly 10%. The overshoot and undershoot of i_1 is almost 100%.

4.3. Controller for smooth transition and simulation

To reduce the overshoot and undershoot of both i_1 and v_o, we designed a new control law by solving the optimization problem (17). By choosing $\eta = 50$ and $w = 1$, $\gamma = 2000$, we obtained an optimized feedback gain K_2:

$$K_2 = \begin{bmatrix} -0.0056 & -0.0007 \\ -0.0001 & -0.0004 \\ -0.1011 & -0.0137 \\ -0.0014 & -0.0065 \\ 0.0204 & -0.0650 \\ -7.8443 & 1.0394 \\ -1.1275 & -7.6319 \end{bmatrix}^T \tag{18}$$

We used this feedback gain for simulation with both the averaged model and the SimPower model. Different values for the reference y_{ref} have been tested. For battery voltage and supercapacitor voltage within a certain range, robust tracking have also been verified. An obvious improvement from K_1 is that both the overshoot and undershoot for i_1, v_o are significantly reduced.

The simulation results are shown in Figs. 4 and 5.

The setup for generating Fig. 4 was the same as that for generating Fig. 2, except that the feedback gain K_1 was replaced with K_2. As compared with Fig. 2, the overshoot and undershoot for v_o was reduced from 10% to less than 5%. The overshoot/undershoot for i_1 were almost all gone. Similar performance improvement can be seen in Fig. 5.

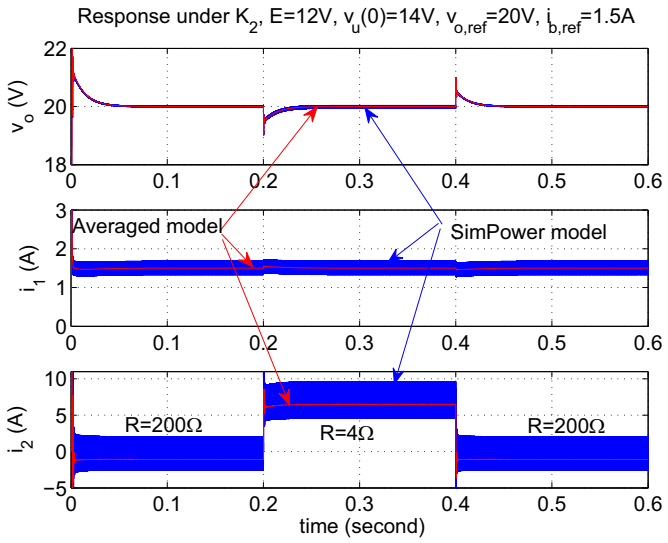

Fig. 4. Response to load switch: $i_{1,\mathrm{ref}} = 1.5$ A, $v_{o,\mathrm{ref}} = 20$ V, feedback gain K_2.

5. Experimental results

The experimental test bench was constructed at a reduced scale, as compared to some real applications. The circuit is described in Fig. 1 and the parameters are given in Table 1. For the battery module, a *Panasonic* LC-R067R2P was selected. The supercapacitor consists of two modules of BMOD0058 MAXWELL 58 F–16.2 V DC in parallel. Same type of MOSFETs were used for the bidirectional buck–boost converters. The controller was implemented with Texas Instruments' TMS320F28335. The switching frequency of the dc–dc converters and the sampling frequency were programmed at 18 kHz. The experiment setup is shown in Fig. 6.

The state feedback control $u = K_2x$ (K_2 provided in (18)) was implemented with a microprocessor. The initial battery voltage was between 12 V and 12.3 V, and the initial supercapacitor voltage was between 13.6 V and 14.8 V. The load was switched between 5 Ω and 360 Ω.

The objective is to track the load voltage v_o and the inductor current i_1, which is very similar to the battery current i_b except with

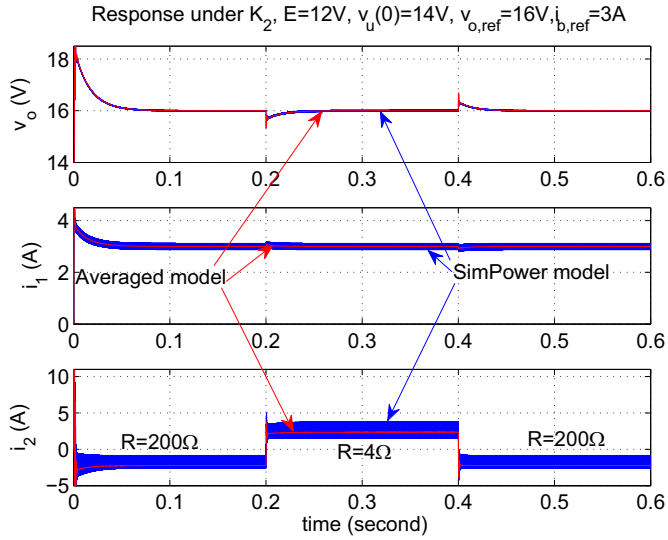

Fig. 5. Response to load switch: $i_{1,\mathrm{ref}} = 3$ A, $v_{o,\mathrm{ref}} = 16$ V, feedback gain K_2.

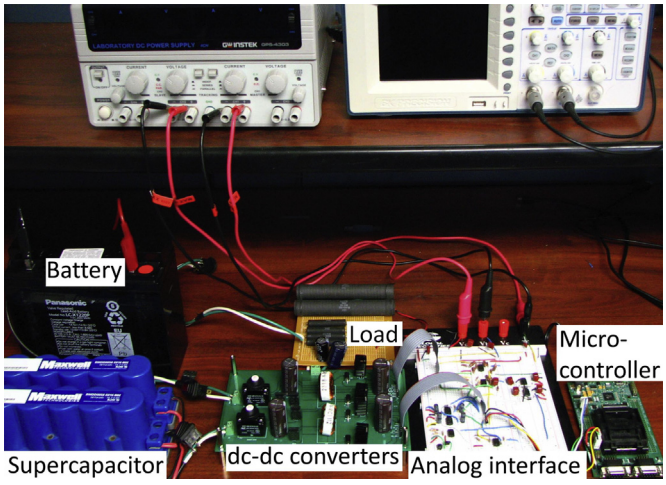

Fig. 6. Experiment setup.

larger ripples. We set the reference for v_o at $v_{o,\mathrm{ref}} = 16$ V, 18 V, 20 V, respectively. For the reference of i_1, we tested two values $i_{1,\mathrm{ref}} = 1.5$ A, 3 A. To verify the robust tracking performance, same controller $u = K_2x$ was used for all tests.

Fig. 7 is the experimental response to the nominal reference $i_{1,\mathrm{ref}} = 3$ A, $v_{o,\mathrm{ref}} = 20$ V. Channel 1 (top, blue in the web version, 10 V/div) is the load voltage v_o. Channel 2 (second from top, red, 2 A/div) is the inductor current i_1 for the battery side boost converter. Channel 3 (bottom, green, 10 V/div) is the supercapacitor voltage. Channel 4 (third from top, orange, 10 A/div) is the inductor current i_2 for the supercapacitor side boost converter. The supercapacitor current i_{sc} is very similar to i_2 but with smaller ripples. The time scale is 1 s/div. Other figures have the same channel layout and scales.

For the initial 3.5 s, the load was 360 Ω. Both i_1 and v_o tracked the set reference values, $i_{1,\mathrm{ref}} = 3$ A, $v_{o,\mathrm{ref}} = 20$ V, except with some ripples and noises. At about 3.5 s, the load was switched to 5 Ω. At about 8 s, the load was switched back to 360 Ω.

There is no visible change in i_1 and v_o after each load switch. In the corresponding simulation results, there are slight overshoots/undershoots in i_1 and v_o (less than 1 V). These overshoots/undershoots seem to be dominated by the ripples and noises in the experimental results.

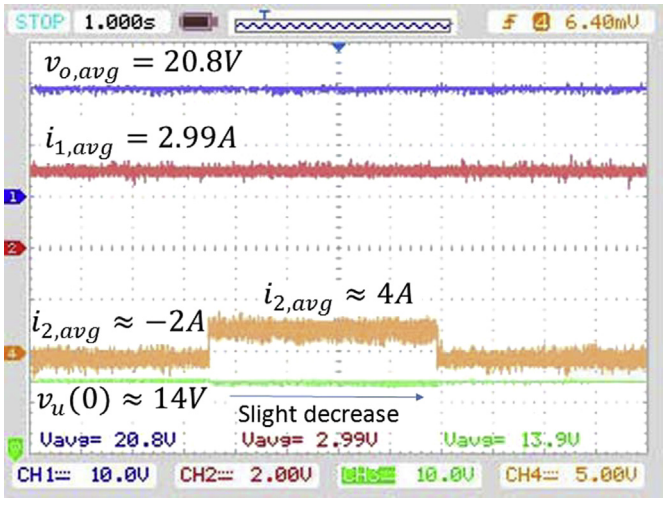

Fig. 7. Tracking response to load switch, $i_{1,\mathrm{ref}} = 3$ A, $v_{o,\mathrm{ref}} = 20$ V, $R = 5$ Ω, 360 Ω.

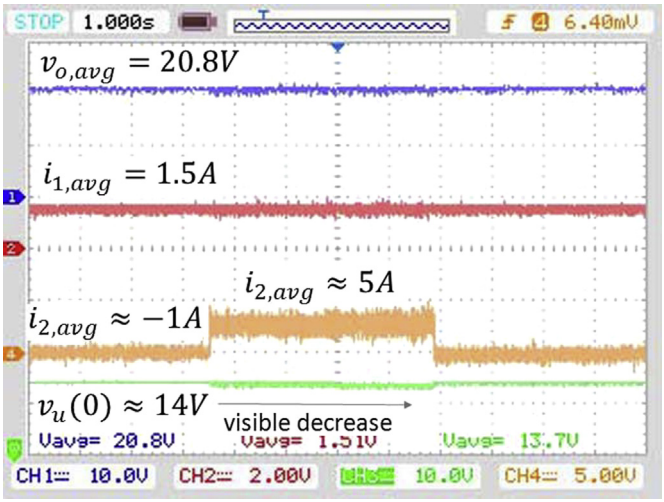

Fig. 8. Tracking response to load switch, $i_{1,\mathrm{ref}} = 1.5$ A, $v_{o,\mathrm{ref}} = 20$ V, $R = 5\ \Omega$, 360 Ω

The load switch is reflected from i_2 (Channel 4). It was negative during light load period and jumps to about 4 A during heavy load period. During heavy load period, the supercapacitor voltage slightly decreases.

This result verifies the robust tracking performance to load switch, and smooth transition for battery current and load voltage, after the load is switched.

To verify the robust tracking performance to different reference values, we obtained the results shown in Figs. 8 and 9.

Fig. 8 shows the tracking response to $i_{1,\mathrm{ref}} = 1.5$ A, $v_{o,\mathrm{ref}} = 20$ V. Both outputs were robustly tracked with smooth transition when the load was switched between 5 Ω and 360 Ω. The difference from Fig. 7 ($i_{1,\mathrm{ref}} = 3$ A) is that the supercapacitor absorbed less current during light load period and supplied more current during heavy load period. This is expected since the role of the supercapacitor is to supply necessary power so that the current from the battery is maintained at a desired value.

The decrease of the supercapacitor voltage during heavy load period is more visible than the case with $i_{1,\mathrm{ref}} = 3$ A. Because of this, the supercapacitor current slightly increased as it was discharged. Another difference from Fig. 7 is that during heavy load period, the ripples and noises of i_1 and v_o were larger. The supercapacitor voltage also had larger ripples.

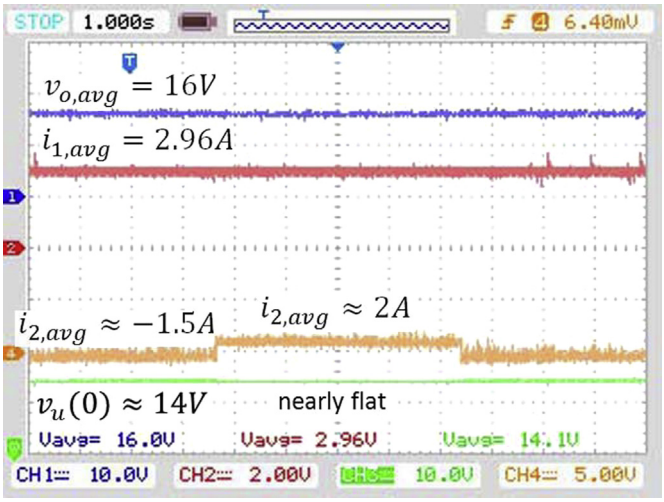

Fig. 9. Tracking response to load switch, $i_{1,\mathrm{ref}} = 3$ A, $v_{o,\mathrm{ref}} = 16$ V, $R = 5\ \Omega$, 360 Ω.

Fig. 9 shows the tracking of $i_{1,\mathrm{ref}} = 3$ A, $v_{o,\mathrm{ref}} = 16$ V. As compared with Fig. 7, the output power demand is smaller so the power supplied by the supercapacitor is reduced, as reflected by the smaller i_2.

We tested other combinations of output reference, battery voltage and supercapacitor voltage and verified that reference tracking can be achieved within a large range of parameters. The tracking responses were very similar. The output voltage and battery current were always around the desired reference values. All the changes of reference values, the source voltages and load resistance were handled by the supercapacitor.

6. Conclusions

We addressed some control design problems for a power system driven by battery/supercapacitor hybrid energy storage devices. The control objectives include tracking the references for two variables in the presence of uncertain conditions and achieving smooth transition during load switch. Based on a newly derived state-space averaged model, the control design problems were converted into optimization problems with LMI constraints. The effectiveness of the control design methods was validated by both simulation and experiment. The results developed in this paper will find possible applications in electric, hybrid and plug-in hybrid electric vehicles, wind systems, photovoltaic systems, and microgrids.

References

[1] S. Fiorenti, J. Guanetti, Y. Guezennec, S. Onori, J. Power Sources 241 (2013) 112–120.
[2] E. Karden, S. Ploumen, B. Fricke, T. Miller, K. Snyder, J. Power Sources 168 (1) (2011) 2–11.
[3] S.M. Lukic, S.G. Wirasingha, F. Rodriguez, J. Cao, A. Emadi, Vehicle Power & Propulsion Conference (VPPC'06), IEEE, September 2006.
[4] G. Sikha, B.N. Popov, J. Power Sources 134 (1) (2004) 130–138.
[5] A.M. Gee, R.W. Dunn, in: 45th International Universities Power Engineering Conference (UPEC), 2010, pp. 1–6.
[6] W. Li, G. Joos, in: Proceedings of the IEEE Power Electronics Specialists Conference, 2008, pp. 1762–1768.
[7] L. Wei, G. Joos, J. Belanger, IEEE Trans. Ind. Electron. 57 (4) (Apr. 2010) 1137–1145.
[8] F. Ongaro, S. Saggini, P. Mattavelli, IEEE Trans. Power Electron. 27 (9) (Sept. 2012) 3944–3952.
[9] M.E. Glavin, P.K.W. Chan, S. Armstrong, W.G. Hurley, in: Proceedings of the IEEE Power Electronics & Motion Control Conference, 2008, pp. 1688–1695.
[10] H. Zhou, T. Bhattacharya, D. Tran, T.S.T. Siew, A.M. Khambadkone, IEEE Trans. Power Electron. 26 (3) (March 2011) 923–930.
[11] P. Thounthong, S. Rael, B. Davat, J. Power Sources 158 (1) (2006) 806–814.
[12] P. Thounthong, S. Rael, B. Davat, J. Power Sources 193 (1) (2009) 376–385.
[13] Z. Yu, D. Zinger, A. Bose, J. Power Sources 196 (4) (2011) 2351–2359.
[14] A.L. Allegre, A. Bouscayrol, R. Trigui, in: Vehical Power and Propulsion Conference, 2009, VPPC'09, IEEE, 2009, pp. 213–220.
[15] J. Cao, A. Emadi, IEEE Trans. Power Electron. 27 (1) (Jan. 2012) 122–132.
[16] M.-E. Choi, S.-W. Kim, S.-W. Seo, IEEE Trans. Smart Grid 3 (1) (March 2012) 463–472.
[17] E. Ribeiro, A.J.M. Cardoso, C. Boccaletti, in: IEEE International Symposium on Power Electronics, Electrical Drives, Automation and Motion (SPEEDAM), 2012, pp. 914–919.
[18] L. Gao, R.A. Dougal, S. Liu, IEEE Trans. Power Electron. 20 (1) (Jan. 2005) 236–243.
[19] S. Lu, K.A. Corzine, M. Ferdowsi, IEEE Trans. Veh. Technol. 56 (4) (July 2007) 1516–1523.
[20] S. Pay, Y. Baghzouz, in: Proceedings of the IEEE Conference on Power Technology, vol. 3, June 2003. Bologna, Italy.
[21] A. Santucci, A. Sorniotti, C. Lekakou, J. Power Sources (2014).
[22] F.S. Garcia, A.A. Ferreira, J.A. Pomilio, in: 24th Annual IEEE Applied Power Electronics Conference and Exposition (APEC), 2009, pp. 826–832.
[23] Y. Kim, J. Koh, Q. Xie, Y. Wang, N. Chang, M. Pedram, J. Power Sources (2014).
[24] R. Carter, A. Cruden, in: International Symposium on Power Electronics, Electrical Drives, Automation and Motion, June 2008, pp. 727–732.
[25] Y. Zhang, Z. Jiang, X. Yu, in: IEEE Energy2030 Conference, IEEE, 17–18 November 2008, pp. 1–6.

[26] H. Jung, C. Conficoni, A. Tilli, T. Hu, American Control Conference, Washington, DC, June 17–19, 2013.
[27] D. Shin, Y. Kim, Y. Wang, N. Chang, M. Pedram, J. Power Sources 205 (2012) 516–524.
[28] T. Hu, H. Jung, J. Power Sources 233 (2013) 14–22.
[29] Y. Yao, F. Fassinou, T. Hu, IEEE Trans. Power Electron. 26 (9) (Sept. 2011) 2614–2626.
[30] T. Hu, IEEE Trans. Power Electron. 26 (2) (Feb. 2011) 399–410.
[31] T. Hu, Z. Lin, Control Systems with Actuator Saturation: Analysis and Design, Birkhäuser, Boston, 2001.
[32] T. Hu, Z. Lin, B.M. Chen, Automatica 40 (2004) 1229–1238.
[33] T. Thibodeau, W. Tong, T. Hu, Automatica 45 (9) (2009) 2046–2051.